https://doi.org/10.17563/rbav.v37i3.1110

3D computational analysis of field emission from hemi-ellipsoidal structures

Análise computacional em 3D da emissão por campo de estruturas hemi-elipsoidais

Hilton Henrique Bertan[1]*, Davi Sabbag Roveri[1,2], Guilherme Mauad Sant'anna[1], Juliano Fujioka Mologni[1,3], Edmundo da Silva Braga[1], Marco Antonio Robert Alves[1]

ABSTRACT

In order to evaluate the electric field associated to field emission, a computational model was elaborated to investigate hemi-ellipsoidal structures. The emitters were simulated as 3D single structures, aiming to establish a relevant methodology for a more complex study.

Keywords: Nanotechnology, Field emission, Numerical simulation, Hemi-ellipsoidal emitter.

RESUMO

Com o objetivo de avaliar o campo elétrico associado à emissão por campo de estruturas hemi-elipsoidais, um modelo computacional foi elaborado para investigação. Os emissores foram simulados em 3D como estruturas isoladas visando estabelecer uma metodologia a ser replicada em estudos mais complexos.

Palavras-chave: Nanotecnologia, Emissão por campo, Simulação numérica, Emissor hemi-elipsoidal.

[1]Universidade Estadual de Campinas – Departamento de Semicondutores, Instrumentos e Fotônica – Campinas (SP) – Brazil
[2]Universidade Federal de Uberlândia – Escola de Engenharia Elétrica – Uberlândia (MG), Brazil
[2]ESSS-ANSYS – Engineering Simulation and Scientific Software – São Paulo (SP), Brazil
Correspondence author: Hilton Henrique Bertan – Universidade Estadual de Campinas –Departamento de Semicondutores, Instrumentos e Fotônica, Cidade Universitária Zeferino Vaz, CEP 13.083-852 – Campinas (SP) – Brazil
E-mail: hiltonbertan@yahoo.com.br
Received: 05/09/2018 **Approved:** 29/11/2018

INTRODUCTION

In the 1950's, vacuum electronic devices were overcome by solid-state microelectronic components. However, research carried out in recent decades revealed that vacuum electronic devices are again competing with solid-state semiconductor devices, but this time using the field emission phenomena[1]. The advantages include: low-cost manufacturing; the ability to operate with high current density at room temperature; endurance to variations in temperature and incident radiation[2]. There are various applications for electron field emitters, namely field emission displays, microwave amplifiers[3] and pressure/displacement sensors[4].

THEORY

The theory related to field emission was firstly studied in 1928 by Fowler and Nordheim[5,6]. The emitted current density J_{FN} (A/cm^2) is related to the electric field on the surface E (V/cm) and to the work function, ϕ (eV), according to Eq. 1, which is also known as the Fowler-Nordheim Relationship (F-N).

$$J_{FN} = \frac{AE^2}{\phi t^2(y)} exp\left(-B\frac{\phi^{3/2}}{E}v(y)\right) \quad (1)$$

where $A = 1.54 \times 10^{-6}$ AeV/V^2; $B = 6.87 \times 10^7$ (VeV)$^{-3/2}$/cm; $y = 3.79 \times 10^{-4} E^{1/2}/\phi$; $t^2(y) = 1.1$; $v(y) = 0.95 - y^2$.

Regarding materials with work function (ϕ) equal to 4.5 eV, the electron emission can be initiated from an electric field intensity E of approximately 10^7 V/cm[7]. The emitted current, I (A), can be calculated by integrating the current density, J_{FN}, over the surface of the emitter S, just as shown in Eq. 2.

$$I = \iint_{emitter} J_{FN}\, dS \quad (2)$$

Due to the elongated geometric shape of the emitter, the electric field E at its apex is significantly higher than the applied macroscopic field F_M. Thereby, the ratio between E and F_M is known as the field enhancement factor[7]: $\gamma = E/F_M$.

Various studies have demonstrated that some geometric shapes present higher γ than others, producing higher current densities with lower anode voltage V_{anode}, which is a characteristic of a good emitter[8]. The importance of studying hemi-ellipsoidal emitters lies on the fact that such structures gather various advantages: high γ; mechanical robustness; low cost manufacturing. Equation 3 describes the field enhancement factor γ at the apex of a hemi-ellipsoidal emitter with height L and base radius ρ[9].

$$\gamma = \frac{\zeta^3}{[\{\alpha\, ln(\alpha + \zeta)\} - \zeta]} \quad (2)$$

where $\zeta = (\alpha^2 - 1)^{1/2}$; $\alpha = L/\rho$.

METHODOLOGY

The numerical simulations were performed using the Ansys-Maxwell software[10], which applies the finite elements method to solve and determine electric field distribution. During the simulations, the electrodes were configured as perfect electrical conductors (PEC) and considered immersed into perfect vacuum.

Some structures were introduced nearby the emitters to improve the mesh refinement in the critical regions of the model. Although these structures were configured as vacuum and did not influence the electric field, they induced the software to increment the mesh density inside the critical regions.

The emitted current I cannot be directly calculated (as shown in Eq. 2) because the emitter is set to zero potential just as the cathode is, which makes it impossible to integrate J_{FN} over the real surface of the emitter. Therefore, the current calculation is made by integrating J_{FN} over a virtual cathode, which consists of a hemi-ellipsoidal surface with negligible thickness, equidistant, and near the emitter real surface. It is important to remind the reader that this new virtual structure just works as a virtual measuring probe.

SIMULATION RESULTS

Firstly, single emitters complying with the following characteristics were investigated: L = 1 µm; ϕ = 5 eV; anode voltage V_{anode} between 0 and 1.2 kV. The base radius ρ was kept constant at 100nm in all simulations; higher values were considered not very effective, since they presented very low aspect ratios (L/ρ) and, consequently, low values of γ. Small values of the base radius ρ were avoided because they resulted in emitters with such high aspect ratios that the analysis could be simplified – the emitters could be studied as if they were CNTs of great height[11]. The structures of the simulated computational model are depicted in Fig. 1. The 3D hemi-ellipsoidal emitter is designed from a revolution of an ellipsoidal arc over its own major semi-axis.

The complete 3D model is presented in Fig. 2. Additionally, the perspective view of the emitter apex can be seen in Fig. 3.

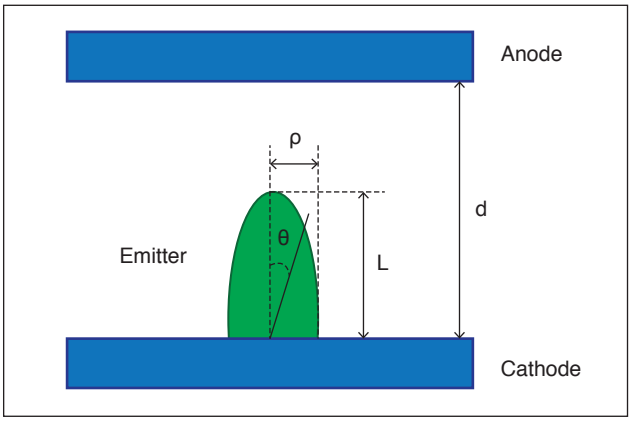

Figure 1: Details of the simulated model.

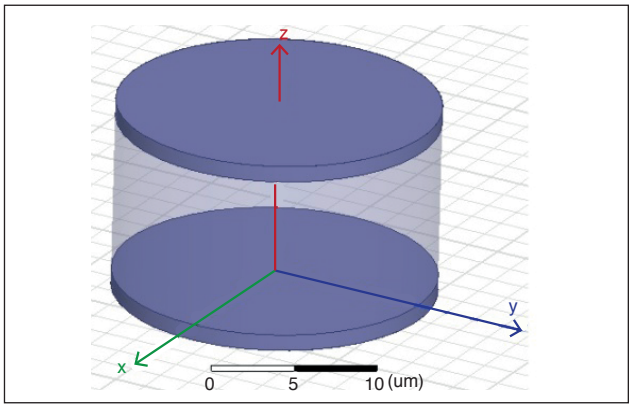

Figure 2: The complete 3D model.

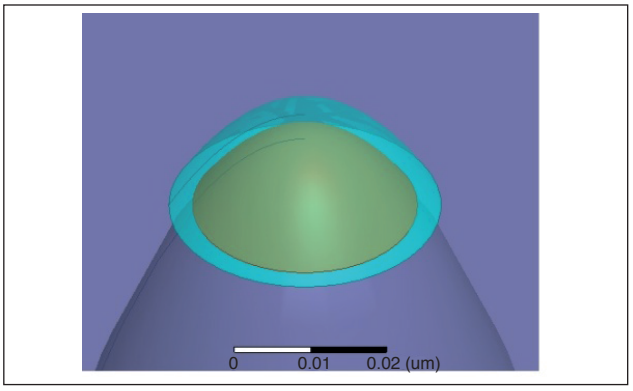

Figure 3: Emitter apex in perspective view.

Still in Fig. 3, the virtual cathode surface is highlighted near the emitter surface. Additionally, the space surrounding both the emitter apex and the virtual cathode is used to confine the mesh operations added manually. This space was set to 5 nm thickness for all simulations. Table 1 describes the dimensions and some simulation parameters.

Table 1: Dimensions and some simulation parameters.

Parameter	Dimension
Anode and cathode radius	10 μm
Anode and cathode thickness	1 μm
L	1 μm
ρ	100 nm
d	10 μm
Virtual probe distance from emitter surface	1 nm

As expected, the closer the virtual probe was from the emitter, the higher were the calculated electric field and enhancement factor. The simulations were performed with the virtual probe positioned at a distance of 1nm from the surface, unlike previous work[12], where the distance used (0.1 nm; interatomic scale) is not suitable for real structures.

The mesh generated in the vacuum region nearby the emitter apex is shown in Fig. 4a, while the mesh generated over the emitter surface is depicted in Fig. 4b. In both figures, it can be noted how the mesh density increases towards the apex – it occurs because this is the region where higher electric field gradients can be found, thereby, this region demands better accuracy than the rest of the model. Figure 5a represents the electric field intensity

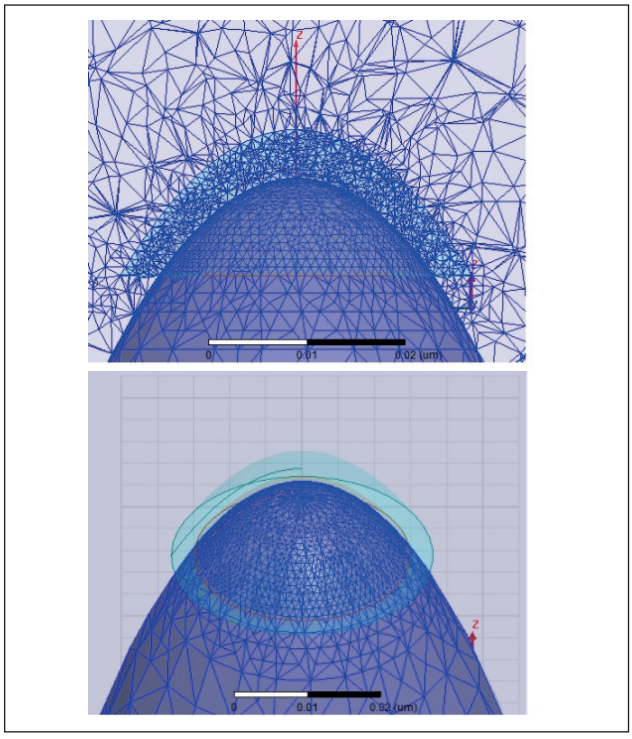

Figure 4: Mesh (A) nearby the emitter and (B) over its surface.

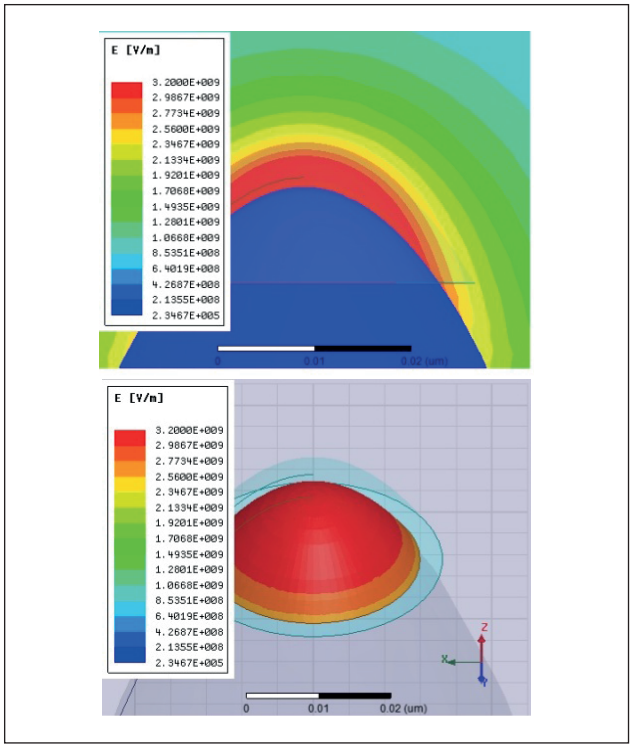

Figure 5: Electric Field intensity (A) nearby the emitter; (B) over the virtual cathode surface.

in the vacuum region surrounding the hemi-ellipsoidal emitter. Additionally, in Fig. 5b, E is represented over the virtual cathode surface.

Using the virtual cathode, the software was able to calculate I as a function of V_{anode}. The result is represented in Fig. 6, where a 1nA current is noted when V_{anode} = 995 V. The 1nA current is used for comparisons in the literature, and often referred to as turn-on current.

Figure 7 correlates E at the emitter apex with the anode voltage V_{anode}. It can be noted that when V_{anode} is 1000 V, the calculated value of E is 4.12×10^9 V/m.

In Fig. 8 the electric field behavior is presented as a function of the hemi-ellipsoid surface emission angle, θ, when V_{anode} = 1000 V.

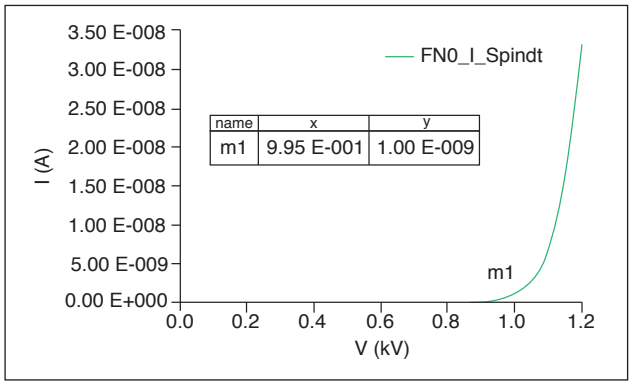

Figure 6: Emitted current (I) versus anode voltage (V_{anode}).

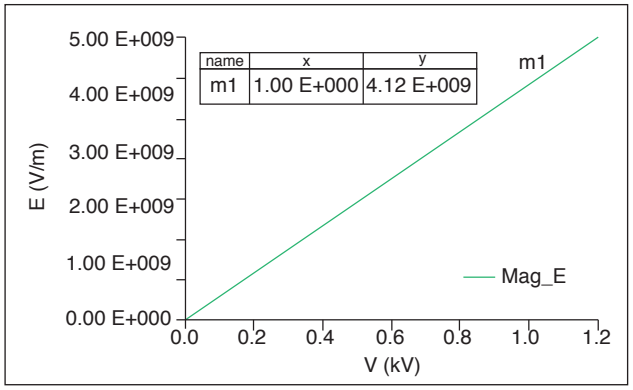

Figure 7: Electric Field (E) versus anode voltage (V_{anode}).

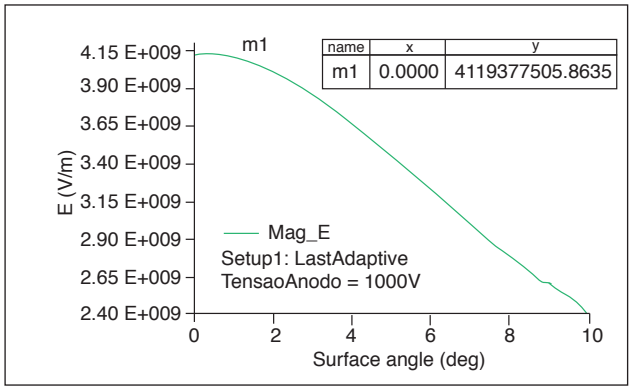

Figure 8: Electric field (E) versus emission angle (θ).

Specifically at the apex (θ = 0°), the electric field magnitude is found to be 4.12×10^9 V/m, which is in accordance with the result highlighted by the marker m1 in Fig. 7.

Considering the value of E at the apex as 4.12×10^9 V/m, through Eq. 1, it is possible to estimate J_{FN} at the hemi-ellipsoidal apex as 7.98×10^6 A/m^2. Since the F-N equation applies to parallel plates, some authors[13] use Eq. 4, which is an adaptation of Eq. 1, to estimate J from protruding emitters positioned over a plane cathode. Equation 4 leads to $J = 1.37 \times 10^7$ A/m^2.

$$J = \frac{1.5 \times 10^{-6}}{\phi} E^2 exp\left(\frac{10.4}{\sqrt{\phi}}\right) exp\left(\frac{-6.44 \times 10^7 \phi^{1.5}}{E}\right) \quad (4)$$

The result presented in Fig. 9 is fundamental to understand the current density distribution over the emitting surface. The figure shows J – calculated using Eq. 4 – as a function of θ, for V_{anode} = 1000 V. The value of J obtained at the apex (θ = 0°) through the simulation is 1.42×10^7 A/m^2, which is similar to those found by Eqs. 1 and 4. The result of Eq. 4 is the closest to the simulation results, as expected, because the F-N formula was originally proposed for plain surfaces.

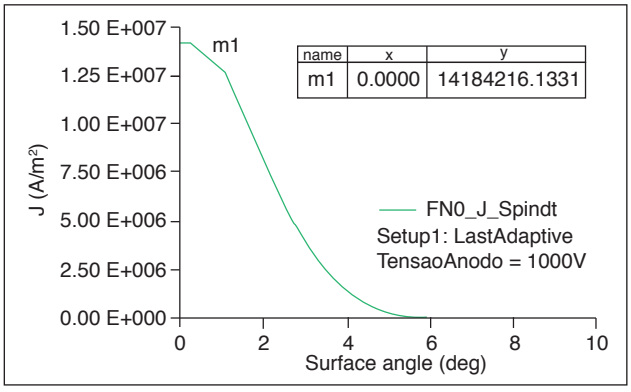

Figure 9: Current density (J) versus emission angle (θ).

It is also possible to estimate the emission area A according to Eq. 5, where I is the turn-on current of 1 nA. The simulation result shows how the emitted current is highly concentrated in a small angle range nearby the emitter apex.

$$A = \frac{I}{J} = \frac{1 \times 10^{-9}}{1.42 \times 10^7} = 7.04 \times 10^{-17} m^2 \quad (5)$$

CONCLUSIONS AND DISCUSSION

A variety of simulation parameters were tested, always looking for a balance between numerical accuracy and available computational resources (like processing time and RAM memory). These tests yielded a satisfactory optimization level[14]. Results of electric field, emitted current and current density were plotted as a function of V_{anode} and θ for a single 3D hemi-ellipsoidal emitter.

The investigations reported hereby have shown that electron emission starts to occur with the expected electric field magnitude. The values of current density calculated by the software through the use of the virtual cathode are in accordance with the results reported in the literature, thereby validating the methodology employed.

This study has shown how the emission phenomenon is highly concentrated in a small emission angle range over the surface. This fact helps to explain the apex destruction reported by some experimental works, because it may lead to overheating under certain operating conditions.

According to this investigation, the 3D modeling of the hemi-ellipsoidal emitter provided results equivalent to the ones obtained previously from 2D simulations of the same emitting geometry, just as expected[15]. In both models, E decreases to approximately 50% of its maximum value when the angle $\theta = 10°$ (Fig.8) and J is reduced to approximately 50% of its maximum value at the apex when $\theta = 2°$ (Fig.9). This decrease in J is so pronounced that the emission of current can be considered negligible from the angle of 6°.

Table 2 compares others parameters obtained for 2D[15] e 3D models.

Table 2: Results for 2D[15] and 3D models.

Parameter	2D[15]	3D	Difference
V_{anode} @I = 1 nA (turn-on current)	1000 V	995 V	0.5%
E @V = 1000V	4.11 × 10^9 V/m	4.12 × 10^9 V/m	0.2%

This work demonstrated that it is possible to use only two-dimensional models, since the differences in the results (V_{anode} and E) obtained from 2D and 3D modeling were very small (< 0.5%). In other words, it was demonstrated that we can substitute three-dimensional models of devices similar to those simulated in this work by 2D structures without significant differences in the final results.

ACKNOWLEDGMENTS

The authors thank the financial support of CNPq and FAPESP. The authors would also like to sincerely thank ESSS for providing cost-free licenses for Ansys Maxwell.

REFERENCES

1. Xu NS, Ejazhuq S. Novel cold cathode materials and applications. Materials Science and Engineering: R: Reports. 2005;48(2-5):47-189. https://doi.org/10.1016/j.mser.2004.12.001

2. Brodie I, Schwoebel PR. Vacuum microelectronics devices. Proceedings of the IEEE. 1994;82(7):1006-1034.https://doi.org/10.1109/5.293159

3. Milne WI, Teo KBK, Amaratunga GAJ, Legagneux P, Gangloff L, Schnell J-P, et al. Carbon nanotubes as field emission sources. Journal of Materials Chemistry.2004;14(6):933-943. https://doi.org/10.1039/B314155C

4. Nicolaescu D. Modeling of the field emitter triode (FET) as a displacement/pressure sensor. Applied Surface Science. 1995;87-88:61-68. https://doi.org/10.1016/0169-4332(94)00530-3

5. Fowler RH, Nordheim L. Electron emission in intense electric fields. Proceedings of the Royal Society of London. 1928;A 119(781):173-181.

6. Spindt CA, Brodie I, Humphrey L, Westerberg ER. Physical properties of thin-film field emission cathodes with molybdenum cones. Journal of Applied Physics.1976;47(12):5248-5263. https://doi.org/10.1063/1.322600

7. Busta HH. Review vacuum microelectronics-1992. J. Micromech. Microeng. 1992;2(2):43-74.https://doi.org/10.1088/0960-1317/2/2/001

8. Utsumi T. Vacuum microelectronics: what's new and exciting. IEEE Transactions on Electron Devices. 1991;38(10):2276-2283. https://doi.org/10.1109/16.88510

9. Forbes RG, Edgcombe CJ, Valdrè U. Some comments on models for field enhancement. Ultramicroscopy. 2003;95:57-65. https://doi.org/10.1016/S0304-3991(02)00297-8

10. Ansys Inc. User's guide – Maxwell 3D, Rev. 5.0. Canonsburg: Ansys; 2011.

11. Roveri DS, Sant'anna GM, Bertan HH, Mologni JF, Alves MAR, Braga ES. Simulation of the enhancement factor from an individual 3D hemisphere-on-post field emitter by using finite elements method. Ultramicroscopy. 2016;160:247-251. https://doi.org/10.1016/j.ultramic.2015.10.018

12. Bertan HH, Roveri DS, Sant'anna GM, Mologni JF, Braga ES, Alves MAR. Estudo e modelamento computacional de emissores de elétrons por efeito de campo de formato hemi-elipsoidal. Revista Sodebras. 2015;10(112)58-63.

13. Zhu W. Vacuum micro-electronics. Hoboken: John Wiley & Sons; 2001.

14. Roveri DS, Bertan HH, Alves MAR, Mologni JF, Braga ES. Use of Ansoft Maxwell software platform for investigation of electrostatic properties of a hemisphere on a post geometry aimed to model field emission devices. ESSS Conference & ANSYS Users Meeting; 2013.

15. Bertan HH, Roveri DS, Sant'anna GM, Mologni JF, Braga ES, Alves MAR. Numerical simulations of electron field emitters based on hemiellipsoid geometry. Journal of Electrostatics. 2016;81:59-63. https://doi.org/10.1016/j.elstat.2016.03.005